Coordination of ScO^+ and YO^+ by Multiple Ar, Kr, and Xe Atoms in Noble Gas Matrixes: A Matrix Isolation Infrared Spectroscopic and Theoretical Study

Yanying Zhao, Yu Gong, Mohua Chen, Chuanfan Ding, and Mingfei Zhou*

Department of Chemistry and Laser Chemistry Institute, Shanghai Key Laboratory of Molecular Catalysts and Innovative Materials, Fudan University, Shanghai 200433, People's Republic of China

Received: August 11, 2005; In Final Form: October 24, 2005

The combination of matrix isolation infrared spectroscopic and quantum chemical calculation results provide strong evidence that scandium and yttrium monoxide cations, ScO^+ and YO^+, coordinate multiple noble gas atoms in forming noble gas complexes. The results showed that ScO^+ coordinates five Ar, Kr, or Xe atoms, and YO^+ coordinates six Ar or Kr and five Xe atoms in solid noble gas matrixes. Hence, the ScO^+ and YO^+ cations trapped in solid noble gas matrixes should be regarded as the $[ScO(Ng)_5]^+$ (Ng = Ar, Kr, or Xe), $[YO(Ng)_6]^+$ (Ng = Ar or Kr) or $[YO(Xe)_5]^+$ complexes. Experiments with dilute krypton or xenon in argon or krypton in xenon produced new IR bands, which are due to the stepwise formation of the $[ScO(Ar)_{5-n}(Kr)_n]^+$, $[ScO(Kr)_{5-n}(Xe)_n]^+$ ($n = 1-5$), $[YO(Ar)_{6-n}(Kr)_n]^+$ ($n = 1-6$), and $[YO(Ar)_{6-n}(Xe)_n]^+$ ($n = 1-4$) complexes.

Introduction

The electronic and geometric structures of transition metal oxides are widely studied.[1−13] The matrix isolation technique played an important role in providing valuable spectral and structural properties of transition metal oxide molecules. Various experimental studies have been performed using different methods for producing transition metal oxide molecules in noble gas matrixes, and the ground states and spectroscopic properties of the transition metal oxide molecules have been determined using infrared absorption and electron spin resonance spectroscopies.[6−13] It is generally assumed that the noble gas matrix that confines the oxide molecules is electronically innocent, that is, the oxide species trapped in the solid matrix can be regarded as isolated "gas-phase" molecules.[14] The vibrational frequencies for most transition metal monoxides trapped in noble gas matrixes are shifted with respect to their values measured in the gas phase by only 10−20 cm^{-1}.[13,14] However, considerable variations in the values of measured vibrational fundamentals in different noble gas matrixes have been observed for some metal oxide species.[15−18] Recent investigations have shown that the vibrational properties of CUO in an argon matrix are very different from those in a neon matrix. The experimental and theoretical results indicated the existence of direct bonding interactions between CUO and noble gas atoms in solid noble gas matrixes.[15,16] Subsequent studies showed that actinide metal oxides such as UO_2 and UO_2^+ trapped in noble gas matrixes are also coordinated by multiple noble gas atoms.[17,18] The UO_2 and UO_2^+ species observed in solid noble gas matrixes should be regarded as the $UO_2(Ng)_n$ and $[UO_2(Ng)_n]^+$ complexes.

In this paper, we report that transition metal oxides also form a variety of noble gas complexes. We will show that the transition metal oxide cations, ScO^+ and YO^+, trapped in solid noble gas matrixes, are coordinated by five or six noble gas atoms in forming the distinct transition metal−noble gas complexes. A preliminary report of the $[ScO(Ar)_{5-n}(Kr)_n]^+$ and $[ScO(Kr)_{5-n}(Xe)_n]^+$ complexes has been communicated.[19]

* Corresponding author. E-mail: mfzhou@fudan.edu.cn.

Experimental and Computational Methods

The experimental setup for pulsed laser ablation and matrix isolation infrared spectroscopy has been described in detail previously.[20,21] Briefly, the Nd:YAG laser fundamental (1064 nm, 20 Hz repetition rate, and 8 ns pulse width) was focused onto the rotating metal oxide targets, which were prepared by sintered metal oxide powders (Sc_2O_3 and Y_2O_3, Shanghai Chemical Reagent Corporation, >99.99%). The ablated metal oxide species were codeposited with Kr/Ar, Xe/Kr, or Xe/Ar mixtures onto a 12 K CsI window for 1−2 h at a rate of approximately 5 mmol/h. Infrared spectra were recorded on a Bruker IFS 113 V spectrometer at 0.5 cm^{-1} resolution using a DTGS detector. Matrix samples were warmed to a certain temperature, quickly recooled, and spectra were taken, then the samples were warmed to a higher temperature than before, recooled, and more spectra were taken.

Quantum chemical calculations were performed using the Gaussian 03 program.[22] The most popular Becke's three-parameter hybrid functional, with additional correlation corrections due to Lee, Yang, and Parr was utilized (B3LYP).[23,24] The 6-311+G* basis set for O, Ar, Sc, and Kr, and the SDD pseudopotential and basis set for Y and Xe were used for the calculations of $[ScO(Ng)_n]^+$ and $[YO(Ar)_{6-n}(Kr)_n]^+$, while the SDD pseudopotential and basis set for all atoms were used for the $[YO(Ar)_{6-n}(Xe)_n]^+$ calculations.[25,26] The geometries were fully optimized; the harmonic vibrational frequencies were calculated with analytic second derivatives, and zero-point vibrational energies (ZPVE) were derived.

Results and Discussion

Infrared Spectra. Experiments were first performed by codeposition of laser-ablated scandium oxides with pure argon at 12 K. The as-deposited matrix sample displayed strong absorptions at 954.8 and 951.8 cm^{-1}, and weak absorptions at 722.5, 889.2, and 976.3 cm^{-1}. The 954.8 cm^{-1} band was previously assigned to the ScO absorption.[27] The 951.8 cm^{-1} band is due to a site absorption of ScO. The 722.5 and 976.3 cm^{-1} bands were attributed initially to the ScO_2 neutral and

10.1021/jp054517e CCC: $30.25
Published on Web 11/25/2005

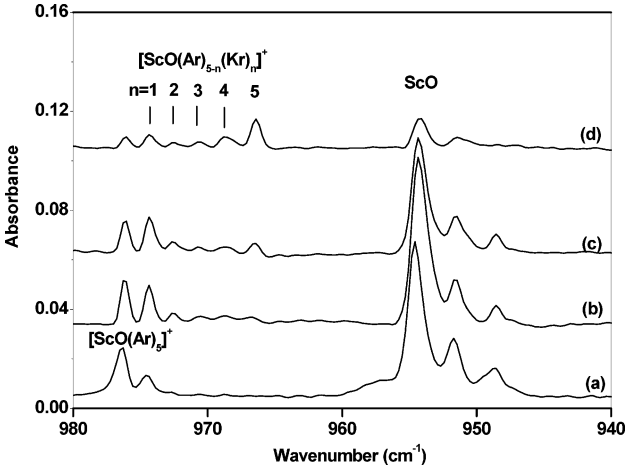

Figure 1. Infrared spectra in the 980−940 cm^{-1} region from codeposition of laser-evaporated scandium oxides with 3% Kr in argon (a) after deposition at 12 K, (b) after annealing to 35 K, (c) after annealing to 40 K, and (d) after annealing to 45 K.

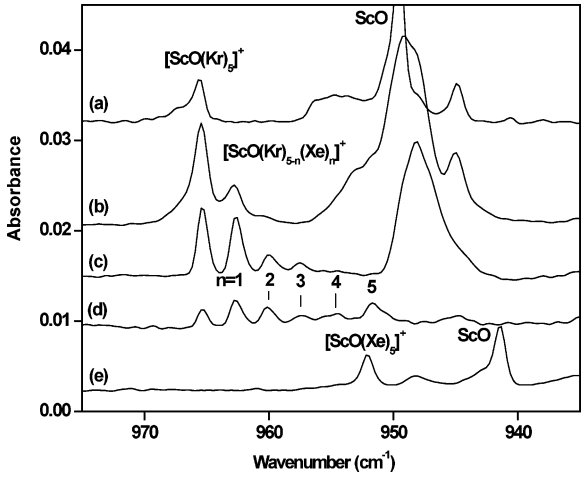

Figure 2. Infrared spectra in the 975−935 cm^{-1} region from codeposition of laser-ablated scandium oxides with noble gases. (a) Pure krypton, after sample deposition at 12 K, (b) 3% Xe in krypton, after sample deposition at 12 K followed by 25 K annealing, (c) after annealing to 46 K, (d) after annealing to 60 K, and (e) pure xenon, after sample deposition at 12 K.

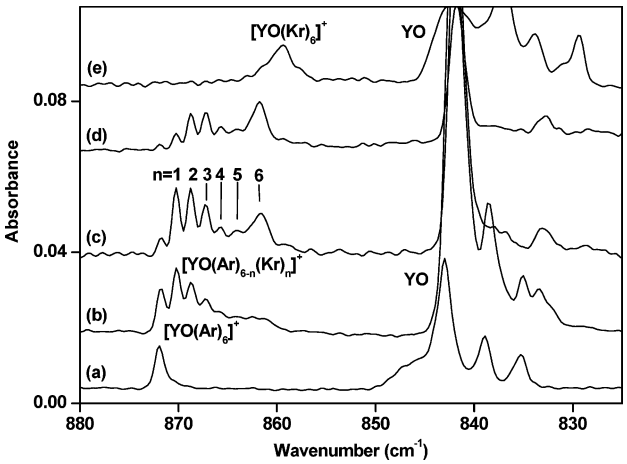

Figure 3. Infrared spectra in the 880−825 cm^{-1} region from codeposition of laser-ablated yttrium oxides with noble gases. (a) Pure argon, after sample deposition at 12 K, (b) 5% Kr in argon, after sample deposition at 12 K followed by 25 K annealing, (c) after annealing to 40 K, (d) after annealing to 45 K, and (e) pure krypton, after sample deposition at 12 K.

the blue site of ScO[27] but have been reassigned later to ScO_2^- and ScO^+, respectively, based upon theoretical calculations and the effects of adding the electron-trapping molecule CCl_4.[28] The ScO, ScO^+, and ScO_2^- absorptions showed no obvious change on annealing. Twenty minutes of broadband irradiation using a 250 W high-pressure mercury arc lamp almost destroyed the ScO_2^- absorption and slightly increased the ScO^+ absorption at the expense of the ScO absorption. The weak band at 889.2 cm^{-1} slightly decreased on annealing, disappeared on broadband irradiation, and has been assigned to the ScO^- anion.[29] The spectrum from codeposition of laser-evaporated scandium oxides with pure krypton exhibited the ScO^+ and ScO absorptions at 965.3 and 949.6 cm^{-1}, respectively.

Experiments were repeated by using mixtures of a lighter noble gas host doped with heavier noble gas guest atoms. Figure 1 shows the spectra in the 980−940 cm^{-1} region from the experiment with a 3% Kr in argon sample. The same product absorptions observed in pure Ar were observed as described above. In addition, five new absorptions at 974.4, 972.5, 970.6, 968.7, and 966.5 cm^{-1} appeared on sample annealing to different temperatures. The peak position of ScO absorption red-shifted by only tenths of wavenumbers upon sample annealing. We assume that only a small part of the argon atoms is lost during the 45 K annealing, as the length of time that the sample was held at 45 K is very short (several seconds). The ScO absorptions decreased significantly upon 45 K annealing, probably due to polymerization to form large ScO clusters. Figure 2 shows the spectra from another experiment with 3% Xe in krypton. The spectra in pure krypton (trace a) and in pure xenon (trace e) are also shown in the figure. A set of new absorptions below the ScO^+ absorption in pure krypton at 962.7, 960.1, 957.6, 954.4, and 951.8 cm^{-1} were produced upon successive annealing cycles, which terminate around the ScO^+ absorption in pure xenon at 952.1 cm^{-1}.

A series of experiments was also performed using a bulk Y_2O_3 target. The infrared spectra in the 880−825 cm^{-1} region with pure argon and krypton, and mixtures of argon and krypton are shown in Figure 3. Spectrum a was taken from the as-deposited sample with pure argon. The 872.0 cm^{-1} band has previously been assigned to the YO^+ cation and the 843.1, 839.1, and 835.3 cm^{-1} bands to the YO neutral in different trapping sites based upon the effects of isotopic substitution in infrared spectra and theoretical calculations.[30] These absorptions were observed at 859.5 and 836.9, 833.5, and 829.3 cm^{-1} in pure krypton, as shown in spectrum e. Spectra b−d illustrate the successive annealing cycles with a 5% Kr in argon sample. Upon annealing, six new bands lying between the YO^+ absorptions in pure argon and in pure krypton evolved at 870.3, 868.8, 867.2, 865.8, 864.3, and 861.8 cm^{-1}. After annealing to 45 K, the lowest peak in the progression became the strongest and approached the absorption of the YO^+ cation in pure krypton at 859.5 cm^{-1}.

Similar experiments were done with Xe in argon, and the spectra in the 880−820 cm^{-1} region using a 3% Xe in Ar are illustrated in Figure 4. A set of five new absorptions at 867.2, 863.1, 859.2, 855.8, and 847.9 cm^{-1} was produced upon successive annealing cycles. The YO^+ cation was observed at 842.6 cm^{-1} in pure xenon. The results are summarized in Table 1.

$[ScO(Ng)_{5-n}(Ng')_n]^+$ ($n = 0-5$). The absorptions at 974.4, 972.5, 970.6, 968.7, and 966.5 cm^{-1} appeared only in the experiment when krypton was doped into argon. These absorptions lie between the ScO^+ absorptions in pure argon and in pure krypton. The intensities of the more red-shifted bands increased, whereas the higher bands of progression decreased

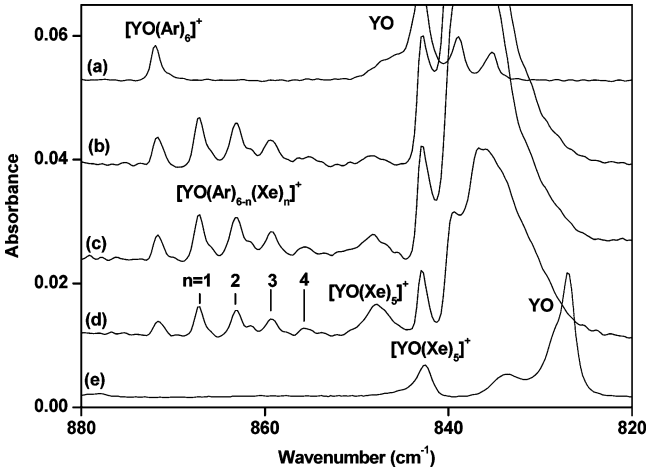

Figure 4. Infrared spectra in the 880−820 cm^{-1} region from codeposition of laser-ablated yttrium oxides with noble gases. (a) Pure argon, after sample deposition at 12 K, (b) 3% Xe in argon, after sample deposition at 12 K followed by 25 K annealing, (c) after annealing to 30 K, (d) after annealing to 35 K, and (e) pure xenon, after sample deposition at 12 K.

TABLE 1: Experimentally Observed M−O Stretching Frequencies (cm^{-1}) for $[ScO(Ng)_{5-n}(Ng')_n]^+$ and $[YO(Ng)_{6-n}(Ng')_n]^+$ in Solid Noble Gas Matrixes

			n						
	Ng	Ng′	0	1	2	3	4	5	6
Sc	Ar	Kr	976.3	974.4	972.5	970.6	968.7	966.5	
	Kr	Xe	965.3	962.7	960.1	957.6	954.4	951.8	
Y	Ar	Kr	872.0	870.3	868.8	867.2	865.8	864.3	861.8
	Ar	Xe	872.0	867.2	863.1	859.2	855.8	847.9[a]	

[a] Y−O stretching frequency for $[YO(Xe)_5]^+$.

when the matrix sample was annealed to higher temperatures step by step. The intervals between the neighboring absorptions are 1.9, 1.9, 1.9, 1.9, and 1.8 cm^{-1}, respectively, which are almost equal. Similar five-band progression with almost equivalent intervals at 962.7, 960.1, 957.6, 954.4, and 951.8 cm^{-1} was also observed in the experiment when xenon was doped into krypton. These experimental observations suggest that ScO^+ is coordinated by multiple noble gas atoms in solid noble gas matrixes. The observation of five distinct new absorptions in both doped experiments strongly suggests that five noble gas atoms are coordinated with ScO^+ in the initial sphere. Hence, the 976.3 cm^{-1} band previously assigned to ScO^+ in solid argon should be reassigned to the $[ScO(Ar)_5]^+$ complex isolated in solid argon, and the 965.3 cm^{-1} band in pure krypton and the 952.1 cm^{-1} band in pure xenon should be assigned to the $[ScO(Kr)_5]^+$ and $[ScO(Xe)_5]^+$ complexes isolated in solid krypton and xenon, respectively. The new absorptions at 974.4, 972.5, 970.6, 968.7, and 966.5 cm^{-1} in solid argon are due to the $[ScO(Ar)_{5-n}(Kr)_n]^+$ complexes (n = 1 to 5) resulting from the successive replacement of coordinated Ar atoms with Kr atoms. Similar absorptions at 962.7, 960.1, 957.6, 954.4, and 951.8 cm^{-1} in the experiment with xenon in krypton are assigned to the $[ScO(Kr)_{5-n}(Xe)_n]^+$ complexes (n = 1 to 5) isolated in solid krypton.

Consistent with the experimental observations, density functional theoretical calculations indicated that ScO^+ could coordinate five noble gas atoms in the first coordination sphere. The calculation results showed that the maximum total binding energy for the $[ScO(Ng)_n]^+$ complexes (Ng = Ar, Kr, or Xe) is achieved when $n = 5$. When $n = 6$, the magnitude of the binding energy decreases, which indicates that binding the sixth noble gas atom is repulsive. The $[ScO(Ng)_5]^+$ complexes were predicted to have C_{4v} symmetry with the equatorial Sc−Ng bond distances shorter than that of the axial Sc−Ng bond (Table 2). The Sc−O stretching frequencies of $[ScO(Ng)_5]^+$ (Ng = Ar, Kr, Xe) were predicted at 1039.9, 1027.3, and 1013.9 cm^{-1}, respectively, which should be scaled by factors of 0.939, 0.940, and 0.939 to fit the observed frequencies (976.3, 965.3, and 952.1 cm^{-1}). On the basis of the calculated frequency (1074.2 cm^{-1}), the yet-to-be-observed gas-phase frequency for ScO^+ is estimated to be around 1010 cm^{-1} with the scale factor of 0.939.

Table 2 presents the calculated geometries, total binding energies, and Sc−O stretching frequencies of the $[ScO(Ar)_{5-n}(Kr)_n]^+$ and $[ScO(Kr)_{5-n}(Xe)_n]^+$ (n = 0−5) complexes. All the possible structural isomers were calculated, and the results are listed in the table. As can be seen, the structural isomers are very close in energy (less than 1.0 kcal/mol difference in total binding energy) with very small (less than 1.0 cm^{-1}) Sc−O stretching frequency difference. We assume that the more strongly bound equatorial atoms were substituted prior to the axial atom. The calculation results (Table 2) indicate that the total binding energy increases monotonically with increasing heavier noble gas atom substitution, while the calculated Sc−O stretching frequencies of the $[ScO(Ng)_{5-n}(Ng')_n]^+$ series exhibit the monotonic red-shift upon successively replacement of lighter noble gas atoms by heavier noble gas atoms. The calculated red-shifts for successively substituting Ar atoms by Kr atoms of the $[ScO(Ar)_{5-n}(Kr)_n]^+$ series are 2.3, 4.9, 7.5, 9.6, and 12.6 cm^{-1}, comparable with the experimentally determined shifts of 1.9, 3.8, 5.7, 7.6, and 9.8 cm^{-1}. For the $[ScO(Kr)_{5-n}(Xe)_n]^+$ series, the calculated red-shifts of 2.9, 4.9, 7.1, 10.5, and 13.4 cm^{-1} are in good agreement with the experimental values of 2.6, 5.2, 7.7, 10.9, and 13.5 cm^{-1}.

$[YO(Ar)_{6-n}(Kr)_n]^+$ (n = 0−6). In the experiment when the laser-evaporated yttrium oxides were codeposited with krypton doped into argon (Figure 3), a six-band progression lying between the YO^+ absorption in pure argon and in pure krypton was evolved on annealing. This suggests that the YO^+ cation is coordinated by six noble gas atoms in solid argon and krypton. Hence, the 872.0 cm^{-1} band previously assigned to YO^+ in solid argon should be reassigned to the $[YO(Ar)_6]^+$ complex isolated in solid argon, and the 859.5 cm^{-1} band in pure krypton should be assigned to the $[YO(Kr)_6]^+$ complex isolated in solid krypton. The new bands at 870.3, 868.8, 867.2, 865.8, 864.3, and 861.8 cm^{-1} in the experiment with krypton in argon are assigned to the $[YO(Ar)_{6-n}(Kr)_n]^+$ complexes (n = 1−6) isolated in solid argon.

Density functional calculations support the above assignment. The total binding energies for the $[YO(Ng)_n]^+$ complexes are shown in Figure 5. We can see that the maximum total binding energy is achieved when $n = 6$ for both argon and krypton. The $[YO(Ng)_6]^+$ complexes (Ng = Ar or Kr) have C_{5v} symmetry with five equivalent equatorial Ng atoms and one axial Ng atom. Table 3 lists the calculated geometries, total binding energies, and Y−O stretching frequencies of the $[YO(Ar)_{6-n}(Kr)_n]^+$ (n = 0−6) complexes. All the possible structural isomers were calculated and the results are listed. Similar to the $[ScO(Ng)_{5-n}(Ng')_n]^+$ complexes, the total binding energy of $[YO(Ar)_{6-n}(Kr)_n]^+$ increases monotonically with increasing Kr atom substitution, while the calculated Y−O stretching frequencies of the $[YO(Ar)_{6-n}(Kr)_n]^+$ series exhibit the monotonic red-shift upon successively replacement of Ar atoms by Kr atoms. The Y−O stretching frequencies for $[YO(Ar)_6]^+$ and $[YO(Kr)_6]^+$ were predicted at 895.8 and 885.9 cm^{-1}, in

TABLE 2: Predicted Geometric Parameters (angstrom), Total Binding Energies (E_b, in kcal/mol), Natural Atomic Charges for Sc (Q_{Sc}), and Sc−O Stretching Vibrational Frequencies (cm^{-1}) of ScO^+ and $[ScO(Ng)_{5-n}(Ng')_n]^+$ (Ng is the Lighter Noble Gas Atom, Ng′ is the Heavier Noble Gas Atom)

		Sc−Ng		Sc−Ng′				
species	Sc−O	equatorial	axial	equatorial	axial	Q_{Sc}	E_b	ν
ScO^+	1.612					1.81		1074.2
$[ScO(Ar)_5]^+$ (C_{4v})	1.632	2.839	3.297			1.55	21.8	1039.9
$[ScO(Ar)_4(Kr)]^+$ (C_{2v})	1.633	2.848, 2.856	3.333	2.939		1.51	24.0	1037.6
$[ScO(Ar)_4(Kr)]^+$ (C_{4v})	1.633	2.847			3.342	1.55	23.0	1037.6
cis-$[ScO(Ar)_3(Kr)_2]^+$ (C_{2v})	1.635	2.865	3.358	2.950		1.46	26.0	1035.0
trans-$[ScO(Ar)_3(Kr)_2]^+$ (C_{2v})	1.635	2.858	3.370	2.951		1.48	26.0	1034.8
$[ScO(Ar)_3(Kr)_2]^+$ (C_{2v})	1.635	2.856, 2.865		2.947	3.369	1.49	25.1	1035.0
$[ScO(Ar)_2(Kr)_3]^+$ (C_{2v})	1.636	2.880	3.401	2.960, 2.959		1.45	28.0	1032.4
trans-$[ScO(Ar)_2(Kr)_3]^+$ (C_{2v})	1.636	2.867		2.960	3.397	1.46	27.0	1033.3
cis-$[ScO(Ar)_2(Kr)_3]^+$ (C_{2v})	1.636	2.876		2.955	3.393	1.47	27.0	1032.4
$[ScO(Ar)(Kr)_4]^+$ (C_{4v})	1.637		3.431	2.970		1.42	29.8	1030.1
$[ScO(Ar)(Kr)_4]^+$ (C_{2v})	1.637	2.887		2.961, 2.969	3.421	1.43	28.9	1030.3
$[ScO(Kr)_5]^+$ (C_{4v})	1.639			2.979	3.433	1.42	30.7	1027.3
$[ScO(Kr)_4(Xe)]^+$ (C_{2v})	1.640	2.988, 3.003	3.478	3.141		1.38	32.7	1024.4
$[ScO(Kr)_4(Xe)]^+$ (C_{4v})	1.641	2.987			3.557	1.39	32.0	1023.3
trans-$[ScO(Kr)_3(Xe)_2]^+$ (C_{2v})	1.641	3.002	3.499	3.163		1.34	34.6	1021.8
cis-$[ScO(Kr)_3(Xe)_2]^+$ (C_{2v})	1.641	3.011	3.495	3.154		1.33	34.6	1023.0
$[ScO(Kr)_3(Xe)_2]^+$ (C_{2v})	1.641	2.999, 3.017		3.149	3.590	1.39	33.9	1022.2
$[ScO(Kr)_2(Xe)_3]^+$ (C_{2v})	1.642	3.028	3.560	3.174, 3.160		1.25	36.4	1020.2
trans-$[ScO(Kr)_2(Xe)_3]^+$ (C_{2v})	1.643	3.012		3.171	3.609	1.25	35.6	1018.9
cis-$[ScO(Kr)_2(Xe)_3]^+$ (C_{2v})	1.643	3.009		3.152	3.630	1.25	35.6	1019.0
$[ScO(Kr)(Xe)_4]^+$ (C_{4v})	1.643		3.584	3.187		1.20	37.9	1016.8
$[ScO(Kr)(Xe)_4]^+$ (C_{2v})	1.644	3.041		3.185, 3.170	3.649	1.21	37.2	1017.6
$[ScO(Xe)_5]^+$ (C_{4v})	1.645			3.197	3.663	1.20	38.7	1013.9

good agreement with the experimentally observed values of 872.0 and 861.8 cm^{-1} (both should be scaled by a factor of 0.973 to fit the experimental values). The YO^+ cation was computed to absorb at 923.7 cm^{-1}. Thus, the yet-to-be-observed gas-phase frequency for YO^+ is estimated to be around 900 cm^{-1}. The calculated red-shifts for successively substituting Ar atoms by Kr atoms in $[YO(Ar)_6]^+$ of 2.1, 3.6, 5.3, 7.3, 7.7, and 9.9 cm^{-1} are also in reasonable agreement with the experimentally determined shifts of 1.7, 3.2, 4.8, 6.2, 7.7, and 10.2 cm^{-1}.

$[YO(Ar)_{6-n}(Xe)_n]^+$ (n = 1−4) and $[YO(Xe)_5]^+$. In the experiment when the laser-ablated yttrium oxides were codeposited with xenon doped into argon (Figure 4), a five-band progression instead of a six-band progression lying between the YO^+ absorption in pure argon and in pure xenon was evolved on annealing. This implies that the YO^+ cation could only coordinate five xenon atoms, and the 842.6 cm^{-1} absorption in pure xenon should be assigned to the $[YO(Xe)_5]^+$ complex. The intervals between the neighboring absorptions are 4.8, 4.1, 3.9, 3.4, and 7.9 cm^{-1}, respectively. It is interesting to note that the interval between the fourth and fifth bands (7.9 cm^{-1}) is about twice as large as the intervals between the other neighboring absorptions. This may suggest that the fifth xenon atom replaces two argon atoms. The 867.2, 863.1, 859.2, and 855.8 cm^{-1} bands are assigned to the $[YO(Ar)_{6-n}(Xe)_n]^+$ complexes with $n = 1-4$, and the 847.9 cm^{-1} band to the $[YO(Xe)_5]^+$ complexes in solid argon.

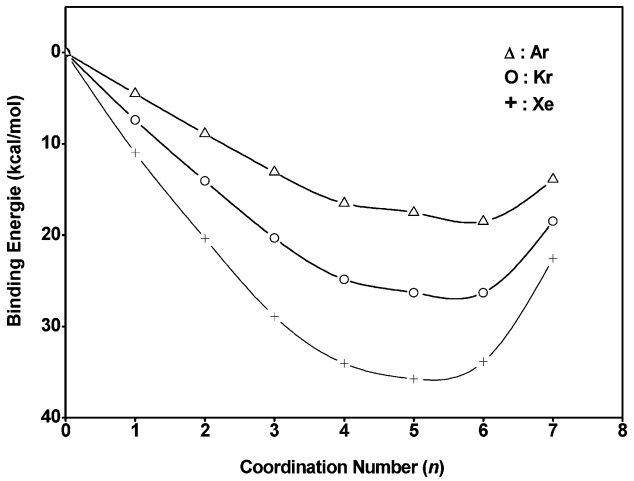

Figure 5. Total binding energy curves calculated for $[YO(Ng)_n]^+$ (Ng = Ar, Kr, Xe) complexes.

In contrast to $[YO(Ar)_n]^+$ and $[YO(Kr)_n]^+$, the calculation results (Figure 5) showed that $[YO(Xe)_5]^+$ represents the optimum coordination of xenon atoms around the YO^+ cation. The calculated geometries, total binding energies and Y−O stretching frequencies of the $[YO(Ar)_{6-n}(Xe)_n]^+$ ($n = 0-4$) and $[YO(Xe)_5]^+$ complexes at the B3LYP/SDD level of theory are listed in Table 4. The calculation also indicated that the total binding energy of $[YO(Ar)(Xe)_5]^+$ is 1.4 kcal/mol lower than that of $[YO(Xe)_5]^+$, thus indicating that replacing two Ar atoms with the fifth Xe atom is energetically beneficial.

The bonding in the above-characterized transition metal−noble gas complexes involves the Lewis acid−base interactions, in which electron density in the Ng lone pairs is donated into vacant orbitals of the metal center. As has been discussed,[19] the 9σ LUMO and 1δ LUMO + 1 molecular orbitals of ScO^+ are metal-based nonbonding orbitals. These orbitals are the primary acceptor orbitals for donation from the noble gas atoms. The HOMO-14 ($6b_2$) and HOMO-17 ($17a_1$) in $[ScO(Ar)_5]^+$ are the resulting bonding orbitals that involve donation from the filled Ar 3p orbitals onto the empty 9σ and 1δ orbitals of ScO^+.[19] The YO^+ cation has similar electronic configuration to that of ScO^+. According to our calculations, the LUMO yttrium-based nonbonding σ orbital of YO^+ is virtually at the same energy level as the 9σ LUMO of ScO^+, but the energy level of the LUMO + 1 yttrium-based nonbonding δ orbitals is about 0.7 eV higher in energy than that of the LUMO + 1 1δ orbitals of ScO^+. Hence, donation from the filled Ar 3p orbitals onto the LUMO of YO^+ dominates the bonding interaction in the $[YO(Ar)_6]^+$ and $[YO(Kr)_6]^+$ complexes. We found that HOMO-20 in $[YO(Ar)_6]^+$ shown in Figure 6 is such a bonding orbital. The interaction between the LUMO +

TABLE 3: Predicted Geometric Parameters (angstrom), Total Binding Energies (E_b, in kcal/mol), Natural Atomic Charges for Y (Q_Y), and Y−O Stretching Vibrational Frequencies (cm^{-1}) of YO^+ and $[YO(Ar)_{6-n}(Kr)_n]^+$ (6-311+G* Basis Set for O, Sc, Ar, and Kr; SDD Basis Set for Y)

		Y−Ar		Y−Kr				
species	Y−O	equatorial	axial	equatorial	aixal	Q_Y	E_b	ν
YO^+ ($C_{\infty v}$)	1.783					2.05		923.7
$[YO(Ar)_6]^+$ (C_{5v})	1.799	3.138	3.556			1.73	18.5	895.8
$[YO(Ar)_5(Kr)]^+$ (C_s)	1.800	3.166, 3.160	3.570	3.186		1.70	20.1	893.7
$[YO(Ar)_5(Kr)]^+$ (C_{5v})	1.801	3.143			3.584	1.71	19.6	893.5
$[YO(Ar)_4(Kr)_2]^+$ (C_s)	1.801	3.205, 3.193	3.587	3.203		1.67	21.7	892.1
$[YO(Ar)_4(Kr)_2]^+$ (C_s)	1.801	3.187, 3.195	3.641	3.209		1.68	21.7	892.3
$[YO(Ar)_4(Kr)_2]^+$ (C_s)	1.802	3.167, 3.171		3.192	3.577	1.68	21.2	891.7
$[YO(Ar)_3(Kr)_3]^+$ (C_1)	1.802	3.253	3.610	3.209, 3.222		1.65	23.1	890.5
$[YO(Ar)_3(Kr)_3]^+$ (C_s)	1.802	3.233	3.599	3.224, 3.225		1.65	23.0	890.5
$[YO(Ar)_3(Kr)_3]^+$ (C_1)	1.803	3.206, 3.188		3.206, 3.207	3.610	1.66	22.7	889.6
$[YO(Ar)_3(Kr)_3]^+$ (C_1)	1.803	3.187, 3.220		3.213, 3.215	3.615	1.66	22.6	888.5
$[YO(Ar)_2(Kr)_4]^+$ (C_1)	1.804	3.724	3.625	3.224, 3.228		1.63	24.5	888.5
$[YO(Ar)_2(Kr)_4]^+$ (C_1)	1.804	3.270, 3.241		3.217, 3.225	3.618	1.63	24.0	888.3
$[YO(Ar)_2(Kr)_4]^+$ (C_1)	1.804	3.241, 3.242		3.224, 3.228	3.617	1.64	24.0	885.9
$[YO(Ar)(Kr)_5]^+$ (C_{5v})	1.804		3.611	3.284		1.65	25.4	888.1
$[YO(Ar)(Kr)_5]^+$ (C_s)	1.805	3.422		3.233, 3.247	3.588	1.61	25.3	886.5
$[YO(Kr)_6]^+$ (C_{5v})	1.805			3.288	3.622	1.63	26.3	885.9

TABLE 4: Predicted Geometric Parameters (angstrom), Total Binding Energies (E_b, kcal/mol), Natural Atomic Charges for Y (Q_Y), and Y−O Stretching Vibrational Frequencies (cm^{-1}) of the $[YO(Ar)_{6-n}(Xe)_n]^+$ Species (SDD Basis Set for All Atoms)

		Y−Ar		Y−Xe				
species	Y−O	equatorial	axial	equatorial	axial	Q_Y	E_b	ν
$[YO(Ar)_6]^+$ (C_{5v})	1.805	3.183	3.545			1.68	22.9	902.5
$[YO(Ar)_5(Xe)]^+$ (C_s)	1.809	3.244, 3.245	3.570	3.295		1.62	27.1	895.8
$[YO(Ar)_5(Xe)]^+$ (C_{5v})	1.810	3.198			3.596	1.63	25.6	895.0
$[YO(Ar)_4(Xe)_2]^+$ (C_1)	1.812	3.307, 3.454	3.640	3.317, 3.318		1.57	30.5	889.4
$[YO(Ar)_4(Xe)_2]^+$ (C_1)	1.813	3.354, 3.340, 3.369	3.650	3.313, 3.314		1.57	30.4	889.2
$[YO(Ar)_4(Xe)_2]^+$ (C_1)	1.813	3.266, 3.278, 3.310, 3.276		3.298	3.646	1.58	29.2	887.0
$[YO(Ar)_2(Xe)_3]^+$ (C_1)	1.817	3.179	3.717	3.302, 3.300, 3.281		1.50	33.9	881.3
$[YO(Ar)_3(Xe)_3]^+$ (C_1)	1.817	3.203, 5.745	3.871	3.276, 3.294, 3.298		1.51	34.4	881.4
$[YO(Ar)_3(Xe)_3]^+$ (C_s)	1.815	3.550	3.646	3.350, 3.351, 3.356		1.52	32.9	882.8
$[YO(Ar)_3(Xe)_3]^+$ (C_1)	1.816	3.292, 3.442, 3.530		3.325 3.331	3.612	1.54	32.1	883.0
$[YO(Ar)_3(Xe)_3]^+$ (C_1)	1.816	3.348, 3.425, 3.359		3.330, 3.339	3.654	1.55	32.1	880.4
$[YO(Ar)(Xe)_4]^+$ (C_{4v})	1.820		3.754	3.323		1.47	36.8	875.7
$[YO(Ar)_2(Xe)_4]^+$ (C_1)	1.820	5.761	4.221	3.312, 3.316, 3.320, 3.323		1.50	37.1	874.6
$[YO(Ar)_2(Xe)_4]^+$ (C_1)	1.818	3.473, 3.585		3.372, 3.373	3.733	1.52	33.8	877.1
$[YO(Ar)_2(Xe)_4]^+$ (C_s)	1.818	3.419		3.356, 3.443	3.717	1.50	33.5	879.3
$[YO(Ar)_1(Xe)_5]^+$ (C_s)	1.822	5.890		3.336, 3.325	3.844	1.38	37.6	867.2
$[YO(Xe)_5]^+$ (C_{4v})	1.823			3.333	3.833	1.38	37.0	871.0

1 of YO^+ and the filled Ar 3p orbitals is not observed in the $[YO(Ar)_6]^+$ and $[YO(Kr)_6]^+$ complexes due to the higher energy level of the LUMO + 1 of YO^+. Consistent with the above notions, the calculated natural atomic charges for the metal center listed in Tables 2−4 decreased upon successively replacement of lighter noble gas atoms by heavier noble gas atoms.

The neutral ScO and YO absorptions are only slightly shifted in the experiments using mixtures of a lighter noble gas host doped with heavier noble gas guest atoms, and no distinct band progression was produced. These experimental observations imply that the neutral ScO and YO molecules do not form stable noble gas complexes in solid noble gas matrixes. Calculations on $ScO(Ar)_n$ ($n = 1$ and 5) almost converged to separated ScO and Ar (Sc−Ar distance larger than 6 Å) with negligible binding energy. The ScO and YO neutral molecules have $^2\Sigma^+$ ground state. The σ LUMO of the cations is singly occupied in the neutrals (SOMO), and the δ LUMO + 1 of the cations becomes the LUMO of the neutrals. These orbitals of the neutrals lie much higher in energy than the corresponding orbitals of the cations, thus the above-mentioned donation interactions are not observed between the neutrals and noble gas atoms.

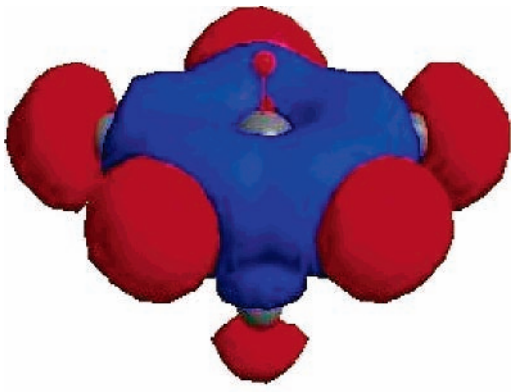

Figure 6. Molecular orbital picture of the $[YO(Ar)_6]^+$ complex.

The present experiments showed that heavier noble gas atoms readily replace lighter noble gas atoms in the coordination sphere of the ScO^+ and YO^+ cations. The calculated binding energies for the $[ScO(Ng)_5]^+$ and $[YO(Ng)_n]^+$ ($n = 6$ for Ar and Kr, $n = 5$ for Xe) complexes are consistent with the experimental observations. The binding energies per Ng atom were computed to be 4.4, 6.4, and 7.7 kcal/mol for $[ScO(Ar)_5]^+$, $[ScO(Kr)_5]^+$, and $[ScO(Xe)_5]^+$, respectively. The binding energies per Ng were predicted to be 3.1, 4.4, and 7.3 kcal/mol for $[YO(Ar)_6]^+$, $[YO(Kr)_6]^+$, and $[YO(Xe)_5]^+$, respectively, slightly lower than those of scandium. These computed binding energies are comparable with those previously reported transition metal−noble gas complexes.[18,31,32]

Conclusions

The combination of matrix isolation infrared spectroscopic and quantum chemical calculation results provide strong evidence that scandium and yttrium monoxide cations, ScO^+ and YO^+, coordinate multiple noble gas atoms in forming noble gas complexes. On the basis of the experiments using mixtures of a lighter noble gas host doped with heavier noble gas guest atoms, the number of noble gas atoms that bind intimately to the ScO^+ and YO^+ cations in the first coordination sphere was determined. The results showed that ScO^+ coordinates five Ar, Kr, or Xe atoms, and YO^+ coordinates six Ar or Kr and five Xe atoms in solid noble gas matrixes. Hence, the ScO^+ and YO^+ cations trapped in solid noble gas matrixes should be regarded as the $[ScO(Ng)_5]^+$ (Ng = Ar, Kr or Xe), $[YO(Ng)_6]^+$ (Ng = Ar or Kr), or $[YO(Xe)_5]^+$ complexes. The Kr and Xe doped experiments produced new absorptions that evolve on annealing, which are due to the $[ScO(Ar)_{5-n}(Kr)_n]^+$, $[ScO(Kr)_{5-n}(Xe)_n]^+$ ($n = 1-5$), and $[YO(Ar)_{6-n}(Kr)_n]^+$ ($n = 1-6$) and $[YO(Ar)_{6-n}(Xe)_n]^+$ ($n = 1-4$) complexes. Density functional calculations showed that distinct $[ScO(Ng)_n]^+$ and $[YO(Ng)_n]^+$ complexes are responsible for the observed trends in frequencies and estimated the binding energies per Ng atom to be 4.4, 6.4, and 7.7 kcal/mol for $[ScO(Ar)_5]^+$, $[ScO(Kr)_5]^+$, and $[ScO(Xe)_5]^+$, and 3.1, 4.4, and 7.3 kcal/mol for $[YO(Ar)_6]^+$, $[YO(Kr)_6]^+$, and $[YO(Xe)_5]^+$, respectively.

Acknowledgment. This work is supported by the NKBRSF (2004CB719501) and NNSFC (20433080) of China.

References and Notes

(1) Huber, K. P.; Herberg, G. *Constants of Diatomic Molecules*; Van Nostrand-Reinhold: New York, 1979.

(2) Merer, A. J. *Annu. Rev. Phys. Chem.* **1989**, *40*, 407.

(3) (a) Wu, H. B.; Desai, S. R.; Wang, L. S. *J. Phys. Chem. A* **1997**, *101*, 2103. (b) Wu, H. B.; Wang, L. S. *J. Phys. Chem. A* **1998**, *102*, 9129. (c) Wu, H. B.; Wang, L. S. *J. Chem. Phys.* **1997**, *107*, 16.

(4) Schroder, D.; Schwarz, H.; Shaik, S. *Struct. Bonding (Berlin)* **2000**, *97*, 91.

(5) Gutsev, G. L.; Rao, B. K.; Jena, P. *J. Phys. Chem. A* **2000**, *104*, 11961.

(6) (a) Weltner, W., Jr.; McLeod, D. *J. Chem. Phys*. **1965**, *69*, 3488. (b) McIntyre, N. S.; Thompson, K. R.; Weltner, W., Jr. *J. Phys. Chem.* **1971**, *75*, 3243. (c) Ferrante, R. F.; Wilkerson, J. L.; Graham, W. R. M.; Weltner, W., Jr. *J. Chem. Phys*. **1977**, *67*, 5904.

(7) Howard, J. A.; Sutcliffe, R.; Mile, B. *J. Phys. Chem*. **1984**, *88*, 4351.

(8) Kasai, P. H.; Jones, P. M. *J. Phys. Chem*. **1986**, *90*, 4239.

(9) (a) Van Zee, R. J.; Hamrick, Y. M.; Li, S.; Weltner, W., Jr. *Chem. Phys. Lett*. **1992**, *195*, 214. (b) Van Zee, R. J.; Hamrick, Y. M.; Weltner, W., Jr. *J. Phys. Chem.* **1992**, *96*, 7247.

(10) Huber, H.; Klotzbucher, W.; Ozin, G. A. *Can. J. Chem.* **1973**, *51*, 2722.

(11) Abramowitz, S.; Acquista, N. *Chem. Phys. Lett.* **1977**, *50*, 423.

(12) Almond, M. J.; Hahne, M. *J. Chem. Soc., Dalton Trans*. **1988**, 2255.

(13) (a) Chertihin, G. V.; Andrews, L. *J. Phys. Chem*. **1995**, *99*, 6356. (b) Andrews, L.; Chertihin, G. V.; Ricca, R.; Bauschlicher, C. W., Jr. *J. Am. Chem. Soc*. **1996**, *118*, 467. (c) Chertihin, G. V.; Bare, W. D.; Andrews, L. *J. Phys. Chem. A* **1997**, *101*, 5090.

(14) (a) Jacox, M. E. *Chem. Soc. Rev*. **2002**, *31*, 108. (b) Jacox, M. E. *Chem. Phys*. **1994**, *189*, 149.

(15) Li, J.; Bursten, B. E.; Liang, B.; Andrews, L. *Science* **2002**, *295*, 2242.

(16) (a) Andrews, L.; Liang, B. Y.; Li, J.; Bursten, B. E. *J. Am. Chem. Soc*. **2003**, *125*, 3126. (b) Andrews, L.; Liang, B. Y.; Li, J.; Bursten, B. E. *Angew. Chem., Int. Ed.* **2000**, *39*, 4565.

(17) Li, J.; Bursten, B. E.; Andrews, L.; Marsden, C. J. *J. Am. Chem. Soc*. **2004**, *126*, 3424.

(18) Wang, X. F.; Andrews, L.; Li, J.; Bursten, B. E. *Angew. Chem., Int. Ed.* **2004**, *43*, 2554.

(19) Zhao, Y. Y.; Wang, G. J.; Chen, M. H.; Zhou, M. F. *J. Phys. Chem. A* **2005**, *109*, 6621.

(20) (a) Chen, M. H.; Wang, X. F.; Zhang, L. N.; Yu, M.; Qin, Q. Z. *Chem. Phys*. **1999**, *242*, 81. (b) Zhou, M. F.; Andrews, L.; Bauschlicher, C W., Jr. *Chem. Rev*. **2001**, *101*, 1931.

(21) (a) Zhou, M. F.; Zhang, L. N.; Shao, L. M.; Wang, W. N.; Fan, K. N.; Qin, Q. Z. *J. Phys. Chem. A* **2001**, *105*, 10747. (b) Zhou, M. F.; Zhang, L. N.; Qin, Q. Z. *J. Phys. Chem. A* **2001**, *105*, 6407.

(22) Frisch, M. J.; Trucks, G. W.; Schlegel, H. B.; Scuseria, G. E.; Robb, M. A.; Cheeseman, J. R.; Montgomery, J. A., Jr.; Vreven, T.; Kudin, K. N.; Burant, J. C.; Millam, J. M.; Iyengar, S. S.; Tomasi, J.; Barone, V.; Mennucci, B.; Cossi, M.; Scalmani, G.; Rega, N.; Petersson, G. A.; Nakatsuji, H.; Hada, M.; Ehara, M.; Toyota, K.; Fukuda, R.; Hasegawa, J.; Ishida, M.; Nakajima, T.; Honda, Y.; Kitao, O.; Nakai, H.; Klene, M.; Li, X.; Knox, J. E.; Hratchian, H. P.; Cross, J. B.; Adamo, C.; Jaramillo, J.; Gomperts, R.; Stratmann, R. E.; Yazyev, O.; Austin, A. J.; Cammi, R.; Pomelli, C.; Ochterski, J. W.; Ayala, P. Y.; Morokuma, K.; Voth, G. A.; Salvador, P.; Dannenberg, J. J.; Zakrzewski, V. G.; Dapprich, S.; Daniels, A. D.; Strain, M. C.; Farkas, O.; Malick, D. K.; Rabuck, A. D.; Raghavachari, K.; Foresman, J. B.; Ortiz, J. V.; Cui, Q.; Baboul, A. G.; Clifford, S.; Cioslowski, J.; Stefanov, B. B.; Liu, G.; Liashenko, A.; Piskorz, P.; Komaromi, I.; Martin, R. L.; Fox, D. J.; Keith, T.; Al-Laham, M. A.; Peng, C. Y.; Nanayakkara, A.; Challacombe, M.; Gill, P. M. W.; Johnson, B.; Chen, W.; Wong, M. W.; Gonzalez, C.; Pople, J. A. *Gaussian 03*, revision B.05; Gaussian, Inc.: Pittsburgh, PA, 2003.

(23) Becke, A. D. *J. Chem. Phys*. **1993**, *98*, 5648.

(24) Lee, C.; Yang, E.; Parr, R. G. *Phys. Rev. B* **1988**, *37*, 785.

(25) (a) McLean, A. D.; Chandler, G. S. *J. Chem. Phys*. **1980**, *72*, 5639. (b) Krishnan, R.; Binkley, J. S.; Seeger, R.; Pople, J. A. *J. Chem. Phys*. **1980**, *72*, 650.

(26) Andrae, D.; Haussermann, U.; Dolg, M.; Stoll, H.; Preuss, H. *Theor. Chim. Acta* **1990**, *77*, 123.

(27) Chertihin, G. V.; Andrews, L.; Rosi, M.; Bauschlicher, C. W., Jr. *J. Phys. Chem. A* **1997**, *101*, 9085.

(28) Bauschlicher, C. W., Jr.; Zhou, M. F.; Andrews, L.; Johnson, J. R. T.; Panas, I.; Snis, A.; Roos, B. O. *J. Phys. Chem. A* **1999**, *103*, 5463.

(29) Zhou, M. F.; Wang, G. J.; Zhao, Y. Y.; Chen, M. H.; Ding, C. F. *J. Phys. Chem. A* **2005**, *109*, 5079.

(30) Andrews, L.; Zhou, M. F.; Chertihin, G. V.; Bauschlicher, C. W., Jr. *J. Phys. Chem. A* **1999**, *103*, 6525.

(31) Wells, J. R.; Weitz, E. *J. Am. Chem. Soc.* **1992**, *114*, 2783.

(32) Sun, X. Z.; George, M. W.; Kazarian, S. G.; Nikiforov, S. M.; Poliakoff, M. *J. Am. Chem. Soc*. **1996**, *118*, 10525.